PCCP

Accepted Manuscript

This is an *Accepted Manuscript*, which has been through the Royal Society of Chemistry peer review process and has been accepted for publication.

Accepted Manuscripts are published online shortly after acceptance, before technical editing, formatting and proof reading. Using this free service, authors can make their results available to the community, in citable form, before we publish the edited article. We will replace this *Accepted Manuscript* with the edited and formatted *Advance Article* as soon as it is available.

You can find more information about *Accepted Manuscripts* in the **Information for Authors**.

Please note that technical editing may introduce minor changes to the text and/or graphics, which may alter content. The journal's standard **Terms & Conditions** and the **Ethical guidelines** still apply. In no event shall the Royal Society of Chemistry be held responsible for any errors or omissions in this *Accepted Manuscript* or any consequences arising from the use of any information it contains.

Physical Chemistry Chemical Physics

ARTICLE

Voltage induced electrochemical reactions in the single lithium-rich layer-oxide nanoparticles†

Tao Li,[1,2] Bohang Song,[1,3] Li Lu[1] and Kaiyang Zeng[1,]*

As the crucial building block of the electrode in lithium-ion battery (LIB), single nanoparticle that responses to an electric field have been rarely characterized experimentally. It is important to study the intrinsic properties of nanoparticles independently, excluding the effects from binder and additives. In this paper, isolated Li-rich layer-oxide ($Li_{1.2}Mn_{0.54}Ni_{0.13}Co_{0.13}O_2$) nanoparticles are studied in comparison with that of the individual Li_2MnO_3 and $LiNi_{1/3}Co_{1/3}Mn_{1/3}O_2$ nanoparticles. The bias triggered changes in morphology and material properties are characterized using dual-frequency scanning probe microscopy (SPM) techniques in ambient air, synthetic air, and Argon atmosphere. Inhomogeneous stiffness/composition is observed on single nanoparticles. The change of local Li^+-ion concentration may contribute to the stiffness variation. The bias induced Li^+-ion redistribution and electrochemical reactions are observed. Nanoparticles are fragmented at high voltage (> 5 V) when excessive amount of Li-ions are removed. This work further demonstrates the application of the multi-frequency SPM techniques on the characterization of nanoparticles for energy storage applications.

1. Introduction

Presently, lithium-ion battery (LIB) holds an undefeatable position for portable electronic devices, and shows great potential for electric vehicles. Many works were dedicated to understanding the kinetic mechanisms of LIB from atomic to macroscopic scales to improve the performance or develop better electrode materials.[1-4] Electrodes are complex composites consisting of active particles, binder and conductive additives.[5] Majority of characterizations for LIB were based on full-cells or half-cells[6-7] or thin film batteries.[8-9] However, the active particles, which are the crucial fundamental elements of the LIBs, are rarely characterized experimentally, especially at the nanoscale. The literatures on the properties of single electrode particles were either based on micro-size particles,[10-11] or simulations (particularly for stress mapping).[12-13] It is therefore necessary and challenge to experimentally study the electrochemical (EC) behaviours of the single nanoparticles to further understand the kinetics of Li^+-ion transportation and phase transformation in host material.

With the emerging of Scanning Probe Microscopy (SPM) technologies, the intrinsic properties of the isolated electrode nanoparticles can be characterized experimentally, without the effects from the binder, additives and mechanical constrains of the hosting materials. In this work, we therefore studied the morphology and property evolutions induced by long-hold electric bias in Li-rich layered-oxide nanoparticles using dual-frequency SPM technique.[14] This technique uses two driving forces to simultaneously excite the cantilever.[15-16] The first flexural resonance is for topography imaging, while the higher flexural resonance is for properties mapping (composition or stiffness).[14] Depending on whether the higher eigenmode is frequency-modulated or operated in open loop, the dual-frequency SPM is categorized as AM-FM or Bimodal-AM, respectively. AM-FM can unambiguously differentiate the conservative and dissipative tip-sample interactions, and quantify elasticity.[17] It is therefore an ideal tool to study the changes of the mechanical properties of the electrode nanoparticles, which is a critical issue for LIB. It is proposed that the contrast in Bimodal-AM can reveal the differences in chemical composition.[18-19] Both techniques are highly sensitive to material property changes and can achieve nanoscale resolution.[17,20] Therefore, the Li^+-ion movement and/or phase transformation in the electrode materials can be postulated from the dual-frequency SPM measurements. The detail working principles of the AM-FM and Bimodal-AM are described in the Section 2.

Li-rich layered-oxide cathode electrode is attractive due to its high energy density (> 250 mAh/g) and high operating voltage (> 3.5 V vs. Li/Li$^+$ in average).[21] It can be considered as a solid solution of $Li_{1+y}M_{1-y}O_2$ or a two-phase mixture as $xLi_2MnO_3\cdot(1-x)LiMO_2$ (M

This journal is © The Royal Society of Chemistry 20xx

Phys. Chem. Chem. Phys., 20xx, **00**, 1-8 | **1**

= Co, Ni, Mn, etc.).[7,22] One of its characteristics is a voltage plateau at ~4.5V during an initial cycle.[21] However, the accompanied irreversible capacity loss and poor rate capability impede its application.[23] To address some of these issues, in this work, the $Li_{1.2}Mn_{0.54}Ni_{0.13}Co_{0.13}O_2$ (LR, also written as $0.5Li_2MnO_3 \cdot 0.5LiNi_{1/3}Co_{1/3}Mn_{1/3}O_2$) nanoparticles were studied in three different environments: ambient air (AA), synthetic air (SA), and Argon (Ar) gas. With the dual-frequency SPM techniques, the electric voltage induced changes in stiffness and/or composition of the nanoparticles can be directly mapped on particle morphology.

2. Materials and SPM Experiments

Synthesis of $Li_{1.2}Mn_{0.54}Ni_{0.13}Co_{0.13}O_2$ (LR) nanoparticles: Particles were synthesized by a spray-dryer assisted sol-gel method. An aqueous solution of 200 mL containing metal acetates with a molar ratio of Mn : Ni : Co equals to 0.54 : 0.13 : 0.13 was slowly dripped into a 300 mL continuously stirred solution that contains 3% excess amount of lithium acetate and with citric acid as chelating agent (same moles as metal ions). The solution was then dried using spray dryer machine (YC-015, Shanghai Politech Instrument & Equipment Co. Ltd). The as-sprayed precursor was further dried again at 80°C for overnight prior to calcination at 800 °C for 15 h.

Synthesis of $LiNi_{1/3}Co_{1/3}Mn_{1/3}O_2$ (NCM) nanoparticles: Particles were prepared from a mixture with the stoichiometric amount of lithium acetate, nickel acetate, cobalt nitrate and manganese acetate that were mixed in distilled water. The mixture was then poured into a distilled water solution of corresponding citric acid with continuous stirring the solution at 70 -100 °C for 5 h. Finally, a red clear viscous gel was obtained as a result of solvent evaporation. The precursor was dried overnight in a vacuum oven at 120 °C. After preheating the dried precursors at 450 °C for 2 h to eliminate organic agent, and calcination at 900 °C for 13 h, the final product was obtained.

Synthesis of Li_2MnO_3 (LMO) particles: Stoichiometric amounts of Li_2CO_3 and MnO_2 were homogenously mixed, and then fired at 900 °C for 15 h to produce Li_2MnO_3 compound.

Sample preparation for SPM characterization: Particles were sonicated in 99% pure industrial alcohol to achieve better dispersion. The suspension was then dripped to a Pt-coated Si wafer. Pt is commonly used as the current collector for commercialized Li-ion batteries.[2] The dispersed particles resided freely on the Pt surface when alcohol was evaporated, leading no mechanical confinement of the isolated particle or cluster of particles. The weak adhesion force between Pt-substrate and particle prevents particle displacement during tapping-mode based SPM scans.

General SPM setup: A commercial SPM (MFP3D-SA, Asylum Research, USA) was used to conduct all of the characterization studies. Conductive probe (AC240TM, Olympus, Japan) was chosen for applying electric field as well as imaging the particle morphology and other properties. The stiffness and inverse optical lever sensitivity of cantilever were calibrated using Sader and thermal noise methods before all imaging. The typical specifications of the probe are listed in Table S2 (Supporting Information). Three types of atmosphere were employed to study the particles responses: ambient air (AA, about 25 °C and 60 % humidity), synthetic air (SA, 21 % oxygen and 79 % nitrogen), and Argon gas (Ar, purity of 99.9997

%). In the controlled atmosphere (SA and Ar), the particles were examined inside a closed cell with continuous gas flow. The inlet pressure of the gas flow is set to about 1.04 bar, at which the cantilever oscillation was minimally disturbed while maintaining the outflow of the gas. The SPM measurements were conducted at least one hours after the continuous gas flow.

Application of electric bias: After locating the particle using Bimodal or AM-FM method (to de described separately in the following sections), a DC bias in 30-second duration was applied to a point on the particle under contact mode via the conductive probe. In this case, the bias-induced changes can reach to large extent, even to the full volume of the particle.[2] During the measurements, tip pressed the particle using about 30 nN force, while the particle was grounded via the Pt-substrate. The magnitude of the applied bias was increased step by step in order to reveal the different responses of particles under long-holding low or high electric field. After each application of the DC bias, the particle was scanned using AM-FM or Bimodal method to obtain both topography and property (stiffness or difference in composition) images.

Compositional imaging by Bimodal-AM: In this technique, the first drive at fundamental cantilever eigenmode works similar to the traditional tapping mode, which was used to acquire the sample topography, amplitude1 and phase1 images. At the same time, the second drive at the higher eigenmode (the third eigenmode in this work) gives an additional set of signals: amplitude2 (A2) and phase2 images. Similar to the first drive, the higher eigenmode is driven with a fixed amplitude and frequency, only without any feedback (open loop). The output signals are free response of the tip-sample interactions. Usually, the second drive amplitude is kept small to prevent severe coupling with the first drive. Under the attractive regime (phase lag > 90°), tip is not in physical contact with the sample surface and long range force dominates in the image contrast. In such nondissipative regime, phase2 was found to be highly sensitive to Hamaker constant variations, which implies that enhanced chemical compositional sensitivity can be achieved.[19,24] When operating under the repulsive regime (phase lag < 90°), in which dissipation has to be taken account, it seems that A2 is more sensitive to the tip-sample force changes than that of the phase2.[20] Thus, A2, phase2 or both can be used to analyze the compositional difference. In addition, recent studies also showed that the contrast inversion was caused by the changes in the ratio of the energy of two eigenmodes.[25-26] In this work, every particle was scanned with the identical setting after every bias application. Thus, contrast inversion is not expected to be a problem. Bimodal AFM was also conducted in all three environments (AA, SA and Ar) to observe the particle behaviours.

Elasticity imaging by AM-FM: Same as the Bimodal-AM, AM-FM also drives with two cantilever eigenmodes simultaneously, except that the higher eigenmode is frequency-modulated (FM). A phase-locked loop (PLL) is included in the control loop for the frequency-modulation. The PLL continuously measures the instantaneous frequency of the oscillation signal and generates an excitation signal at this frequency as a feedback to the control loop. It maintains a 90° phase difference between the response and drive, and thus ensures that the eigenmode always oscillates at its actual resonance frequency.[17] The PLL can operates in two different ways: constant excitation (CE) and constant amplitude (CA). CE mode keeps the excitation amplitude constant, while CA mode keeps the oscillation amplitude constant by adjusting the drive amplitude accordingly.[17] In case of the CA mode that was used in this work, the frequency shift and drive amplitude are directly related to the conservative and dissipative interactions, respectively.[27] FM outputs

two types of data, the frequency and drive amplitude. The frequency image can be further converted to tip-sample contact stiffness (N/m) with proper calibration of the cantilever, or to elastic modulus (GPa) through the contact mechanics models. As the primary usage of the AM-FM in this work is to quantify the elasticity mapping, it has to operate in the repulsive regime to achieve certain indentation to the sample surface. Hence, the drive voltage is set to 2 V for the fundamental eigenmode, and 10 to 20 mV for the third eigenmode. This small amplitude of FM mode prevents the perturbation to the 1st eigenmode cantilever dynamics. Due to the limitation of the SPM set-up, the AM-FM mode can only be performed in AA environment.

Current measurement by Conductive-AFM (Atomic Force Microscopy): In this experiment, bias was applied from the Pt layer of the substrate, and the conductive tip was grounded. Current was measured when tip was in firm contact with the particle. The loading force was about 90 nN. Bias was applied in the same way as that to measure the stiffness and compositional contrast, i.e., holding at a constant voltage for 30 seconds. Before the application of a voltage, a 3-second zero-bias response was applied in order to acquire the equipment noise level as a reference.

3. Results and Discussions

3.1 Semi-quantitative Stiffness Mappings of Pristine Li-rich Nanoparticles

Taking the advantage of the ultrahigh sensitivity to material properties of the higher eigenmode in dual-frequency SPM, the inhomogeneity of three pristine LR nanoparticles is clearly revealed (Fig.1). The particles were scanned by both AM-FM and Bimodal-AM modes in AA with the same tip and identical parameters in the repulsive regime (phase1 < 90°), therefore the relationship between the two modes can be established. AM-FM stiffness (k^c, Fig.1a) and Bimodal-AM amplitude2 (A2, Fig.1b) show nearly identical contrast when the colour scale of Fig.1b is inverted. This observation is consistent with the simulation results for low A2.[25] This indicates that the responses from AM-FM and Bimodal-AM are correlated with inverse contrast in the repulsive regime and are initiated from the same tip-sample interactions. The inhomogeneous contrast of each particle in k^c and A2 may originate from the two microconstituents: Li_2MnO_3 (LMO) and $LiNi_{1/3}Co_{1/3}Mn_{1/3}O_2$ (NCM), of the LR layered-oxide nanoparticles. The X-ray diffraction pattern of LR particles confirms the presence of both phases and the $LiMn_6$ ordering within LMO-like phase (the weak peaks between 21° and 25°, Fig.S1 – Supporting Information).[28] In Fig.1a, each particle has softer (green colour) and stiffer (red colour) domains. The estimated ratio of the reduced elastic modulus *(E)* of the tip-sample system between these domains is about $E_{stiff}/E_{soft} = (k^c_{stiff}/k^c_{soft})^{3/2} = 2.02$, based on Hertzian contact model (Table S1 – Supporting Information).[29-30] These domains may represent the short range ordering of cations and the different Li^+-ion concentration. The domains are randomly distributed on particle surface. LMO-like and NCM phases have fully compatible layered structures, but the former has excessive Li^+-ions in the transition metal (TM) layer.[28] The excess Li^+-ion can ease the tension among anions and strengthening the bonding. In the nonstoichiometric materials, decreased bonding length corresponds with increased elastic modulus.[31-32] Thus, the stiffer domains are expected from the LMO-like phase. To verify this, the average elasticity of individual LMO

and NCM particles were measured by AM-FM method (Table S1 – Supporting Information). Taking the Pt-substrate as a reference (should be the same for all samples), the average ratio of the reduced elastic modulus is $E_{LMO}/E_{NCM} = 1.20$. LMO is slightly stiffer than that of NCM. Considering the perfect structural compatibility between LMO and NCM, the higher E_{LMO} may be due to its higher Li^+-ions concentration and better cation ordering. The positive relationship between Li^+-ion concentration and *E* in layered electrodes has been demonstrated in the simulation of the delithiated/lithiated $LiCoO_2$[33] and nanoindentation studies on polycrystalline $LiCoO_2$ pallet.[31] Nevertheless, when NCM and LMO are fused into a single LR nanoparticle, the ratio of *E* increases from 1.20 to 2.02 because of the LMO domains become stiffer ($E_{Pt}/E_{LMO} = 0.93$), while the NCM domains become softer ($E_{Pt}/E_{NCM} = 1.87$). In this case, NCM and LMO structures are integrated in particular planes of $(003)_R$ and $(001)_M$ so that the relative crystal orientation is fixed.[34] The E_{LMO}/E_{NCM} can be reduced when it is averaged over particles with different orientations.
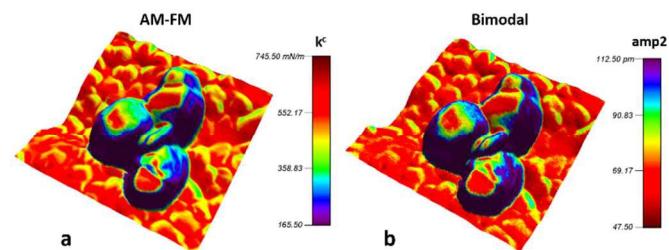

Figure 1. Three-dimensional images of pristine LR particles laid on Pt-substrate scanned by AM-FM and Bimodal-AM methods. Both methods were scanned under repulsive regime (phase1 < 90°). The contact stiffness k^c (a) and amplitude2 (A2) (b) were mapped on the topographic images. Colour scale of figure (b) was inverted so that k^c and A2 show nearly identical contrast. The dramatic stiffness drop along the circumference wall of each particle may be due to the slipping contact between the SPM tip and the particle. Thus, it was not considered in the analysis. Only the central flat regions were analysed throughout this study.

3.2 Positive Electric Field Induced Li-ion Redistributions and Electrochemical Reactions in Li-rich Nanoparticles in Ambient Air

When a pristine particle is subjected to an electric field, Li^+-ion redistribution can be triggered via electromigration, electrochemical (EC) reaction and/or phase transformation.[35] At low voltage, electromigration dominates,[36] but other mechanisms may take place at high voltage. Fig.2 shows typical responses of LR nanoparticle to long-hold positive voltages. Lower bias can cause electromigration by repelling the Li^+-ions away from the contact point but may not sufficiently activate the EC reaction. When the bias is removed, the Li^+-ion relaxation may occur via diffusion driven due to the electric-field induced concentration differences. There is about 30-second time interval between bias application and AM-FM scan (for mode switching and adjusting parameters), this allows the Li^+-ion relaxation. Thus, the changes observed from AM-FM scans should be under quasi-equilibrium conditions. Obvious changes in both topography and stiffness of the nanoparticle are observed after being applied with 2 V bias (Figs.2b to 2c). In order to correct the effects

This journal is © The Royal Society of Chemistry 20xx

Phys. Chem. Chem. Phys., 20xx, **00**, 1-8 | **3**

from tip blunting due to continuous tip wear, the Pt-substrate was used as a reference for stiffness comparison (Fig.S2 – Supporting Information). Height of the particle is reduced while stiffness is also reduced at the regions surrounding the centre (red spot). The electric field under SPM tip is not uniform, especially when the material is inhomogeneous. The field is the strongest at the contact point, and gradually fades further away. Thus, the relatively low field may only repel the positively charged Li^+-ions and reduces the local stiffness. In addition, staggered steps are observed at the edge of the particle. Electric bias induced steep Li+-ion concentration gradient can lead to stress from lattice mismatch. These steps may be the slip planes due to the stress relaxation after removing the voltage, in which dislocations move from the centre towards the edge of the particle.[2] When applied voltage is increased to above 2.5 V (Figs.2e to 2f), EC reaction may be activated such that Li^+-ions are removed from Li-layer in NCM phase. Under the positive voltage, Li^+-ion moves towards the contact point, while electrons flow via the external circuit in the same direction. This behaviour leads to a locally increased stiffness at the centre of particle where the highest electric field is applied. The dramatic changes of the nanoparticle start from 4.5 V (Figs.2g to 2h). This voltage actually corresponds to the voltage plateau in the 1st charging/discharging curve of the LR materials [Fig. S1(b) – Supporting Information]. At this voltage, LMO nanodomains can be activated, leading to phase transformation and massive Li^+-ions extraction from the nanoparticles.[28,37] For LMO, it can easily transform into spinel structure because of dual removals of Li and O ions, whereas the transformation for NCM is difficult since this process must be accompanied with a relocation of transition metals from the transitional metal layer to Li layer. The E_{high} /E_{low} is half of that of the pristine particle and the stiffness homogeneity is increased. Under AA condition, the particle is covered by a thin layer of water molecules and forms meniscus at the tip-sample contact, which can be a Li^+-ions reservoir (Fig.2m).[35-36] Hence, Li^+-ions can escape from the particle surface when sufficient electric energy is supplied. This setup renders the tip-electrode system reversible.[2] The abrupt drop of stiffness on the particle surface may be due to the deintercalation of Li^+-ions in layered structure and/or phase transformation to spinel-like structure near the surface of the particle.[33,38] Particle also expands in both lateral and vertical directions. Further increase of the bias to 5 V leads to the particle fragmentation (Figs.2i to 2j). The particle seems "melted" to the substrate, and become much smaller at 5.5 V (Figs.2k to 2l). The high-voltage hold can result in the phase transformation accompanied with oxygen evolution,[21,39] which may cause the gradual fracture and volume reduction of the LR nanoparticle. The dramatic morphology change seems to occur at the particle surface, and the newly-exposed central core of the particle still shows higher stiffness.

Current profiles observed under different voltage hold (I-V curve) by conductive-AFM are shown in Figs.3a to 3b. Because the bias was supplied via the Pt-substrate, negative voltage is required to maintain the same electric field direction as the tip-biased case. Low current is observed at - 2.5 V (smaller than 10 nA). This may correspond to the EC reaction of NCM phase with deintercalation from Li-layer. The magnitude of the current increases with increased applied bias. At - 4 V, high current peaks are observed in the magnitude of hundreds nA. The current is randomly on-and-off during the voltage hold (Figs.3b to 3c). The high current peaks may be caused by the intermittent activations of LMO-like domains that may lead to extensive electron and/or ion flows. The current initiation voltage (- 2.5 V) and the high current voltage (- 4 V) matches well with the voltages at which the significant changes in morphology (Fig.S3 – Supporting Information) and stiffness image (Fig.2h).

To further investigate the role of LMO-like phase in LR nanoparticles, pure NCM nanoparticles were examined by the same method in AA. The NCM particles can remain integrity at 6 V and different patterns of morphology and property changes are observed (Fig.S4 – Supporting Information). Thus, the fragmentation of the LR nanoparticle by long-hold voltage above 4.5 V is directly caused by the presence of LMO-like phase in the LR nanoparticles. Once LMO-like phase is activated, phase transforms from *C2/m* to spinel-like structure, involving massive removal of Li^+ and O^{2-}-ions. This transformation produces large lattice strain and/or oxygen vacancies that may cause the breakdown of the parent lattice.[21,40] However, the pure LMO particles show no obvious morphology and property changes even at 8 V in AA condition (Fig.S5 – Supporting Information). Thus, the nano-size LMO-like domains that fused into the NCM phase in LR nanoparticles may play a critical role. In addition, the current profiles (Figs.3c to 3d) clearly reflect the different EC reaction mechanisms of LR and NCM nanoparticles during the voltage-holding, respectively. Similar to the case of negative bias, positive bias also generates randomly on-and-off current peaks for LR nanoparticle (Fig.3c). Among these current peaks, lower current maintains at about 1 to 6 nA. High current can only be observed when bias ≥ 4 V. In contrast, NCM nanoparticle only shows lower current (2 to 8 nA) at high voltage, with smooth and continuous profile (Fig.3d). These observations imply that more complex reaction mechanisms are involved in the LR nanoparticle. High current indicates large amount of Li^+-ions movement. These Li^+-ions can be removed from the LMO-like domains during phase transformation. Random LMO-like nanodomains may be activated one by one or as clusters. These nanodomains may also act as solid electrolyte constituents to facilitate Li^+-ions transportation through the structure.[28] The multiple current peaks are most likely associated with the activations of the LMO-like phase. The NCM phase contributes only with smaller current that the magnitude is similar to that of the pure NCM particle.
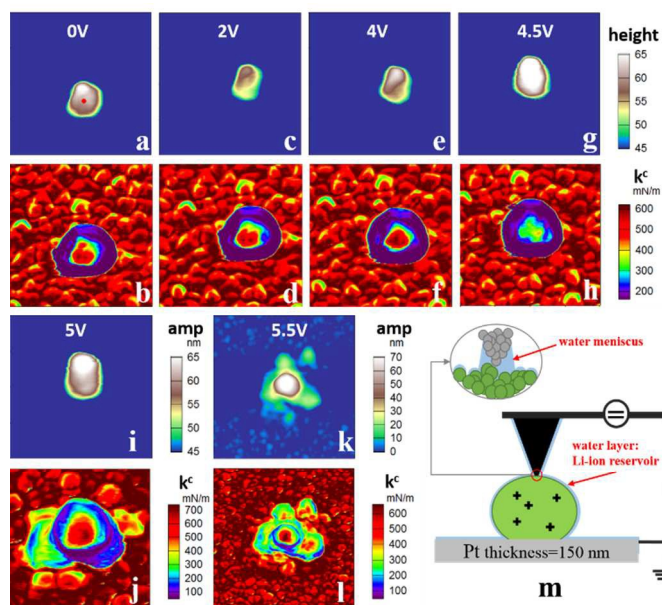

Figure 2. Morphology and contact stiffness k^c evolutions of a typical LR nanoparticle triggered by escalating long-hold positive DC voltages (0 to 6 V) in ambient air (AA). The increment of the voltage was 0.5 V at each step. After each bias application, the particle was

scanned by the AM-FM method. Each bias was applied at the middle surface of the particle for 30-second. Slight thermal drift is unavoidable. The color representation for the amplitude and k^c from 0 to 4.5 V is identical and indicated by the color scale bar on the right side of image "g" and "h". Scan size is 400×400 nm^2 for all of the images, except for "k" and "l" (800×800 nm^2). Same as in Figure 1, the analysis is only focused on the central flat regions of the particle. The tip-particle experimental setup in AA condition is illustrated in "m".
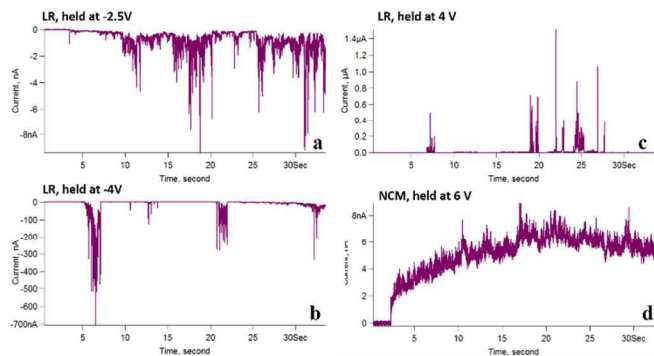

Figure 3. Current profiles observed from LR and NCM particles in ambient air condition by conductive-AFM method. In this case, bias is applied from the Pt-substrate while tip is grounded. Thus, the electric field generated by the negative bias from Pt-substrate corresponds to the positive bias applied via conductive tip, and vice versa.

3.3 Li-rich Nanoparticles Response to Positive Electric Field in Controlled Environments: Synthetic Air and Ar Gas

In AA atmosphere, water, O_2, CO_2 and other impurities complicate the EC reactions and the interpretation of the responses in LR nanoparticle. Thus, the same batch of LR nanoparticles was examined in synthetic air (SA) to exclude the moisture effects. A significant difference is that the particle remains integrated even after being applied with 8 V (Fig.4, image contrast is corrected by Pt response in Fig.S6 – Supporting Information). Only localized deformation and material property variations are observed at high voltage, e.g., the green spot (Fig.4j). This implies that the shattering of LR nanoparticle is attributed to the presence of water molecules in AA. Without this reservoir, it is difficult for Li$^+$-ions to escape and they are preferably trapped inside the nanoparticle. In other words, the water layer facilitates the EC reaction of the nanoparticle, and leads to the substantial Li$^+$-ions extraction and oxygen evolution, which makes the LR particle highly unstable under high voltage in air. Thus, in humid atmosphere, the LR electrode in LIB can be sabotaged even by minor leakage of water molecules. In SA, Li$^+$-ions concentration in nanoparticle can still be changed by voltage and this may lead to local lattice deformation. Electric field mainly induces electromigration rather than EC reactions at the interface, except that certain lithium extraction and formation of metallic lithium can occur at sufficiently high voltages.[2] O_2 may also be involved in the nanoparticle reactions at high voltage, which produces the distinct feature (the elliptical green region surrounded by red ring at 8 V) that is only observed in SA.

Comparing to SA, Ar atmosphere further excludes O_2, and EC reactions are highly impeded. Particle fracture and dramatic volume change were not observed at 8 V, but the localized changes in

particle properties still present (Fig.5, image contrast is corrected by Pt response in Fig.S6 – Supporting Information). In this case, any changes in the nanoparticle should be attributed to the intrinsic responses to the externally applied constant voltage hold. Higher A2 (Figs.5h to 5n) of nanoparticle than that of Pt indicates that the nanoparticle is generally softer than Pt-substrate according to the opposite contrast between AM-FM and Bimodal-AM operated under the repulsive regime, same as the case in AA (Fig.1). After the applications of biases, height and stiffness are inversely related, i.e., when height increases, stiffness decreases, and vice versa. In the perspective of Li$^+$-ion concentration, lower concentration leads to lower stiffness, and the resultant larger repulsive force among anions may lead to expansion of lattice. Obvious property changes at region-A (Fig.5) occurs at 4 and 4.5 V, at which stiffness suddenly decreased and increased, respectively. Similar to AA, 4.5 V is a critical voltage that intensive reactions occur inside the LR nanoparticles. The cyclic change of the local stiffness is similar to that in AA. LR particle intrinsically has more Li$^+$-ions available for charging/discharging cycles. Certain amount of Li$^+$-ions must be maintained inside the particle, otherwise particle will suffer from dramatic mechanical failure such as fracture. LMO-like nanodomains can be activated to achieve higher capacity, but the numbers of these nanodomains need to be carefully controlled to ensure durability. Furthermore, it should be noted that the particle size may also have an effect. Electric field does not vary much when a constant bias is applied to different size of nanoparticles. Small pristine particles tend to be fractured under high positive bias in AA. They holds limited amount of Li$^+$-ions, which can be easily drained under long-hold high voltage. Under the same circumstance, large particle (e.g. diameter > 500 nm) may not be shattered in AA.
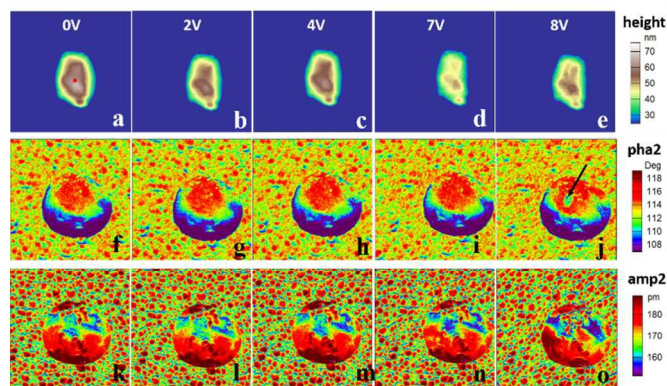

Figure 4. Topography and compositional variations of the LR nanoparticle observed by Bimodal-AM (phase1 > 90°) in synthetic air. Bias (2 to 8 V with 1 V increment) was applied in the middle of the particle. Scan size is 900×900 nm^2. Phase2 and A2 images were corrected by a factor to maintain the same mean value of Pt-substrate throughout.

3.4 Negative Electric Field Induced Reactions of Li-rich Nanoparticles in Ambient Air

The negative-bias induced reactions of LR nanoparticles were also studied in AA. Low negative bias attracts Li$^+$-ion towards the tip-sample contact via electromigration and relaxation can occur via

diffusion after removing the bias. EC reactions can also be triggered, indicated by the high current peaks (> 1.2 μA) observed at 4 V (Fig.3c, positive bias from Pt-substrate corresponds to the negative

bias from tip), at which the dramatic particle expansion occurs (Fig.6). The lack of current and no significant morphology change at
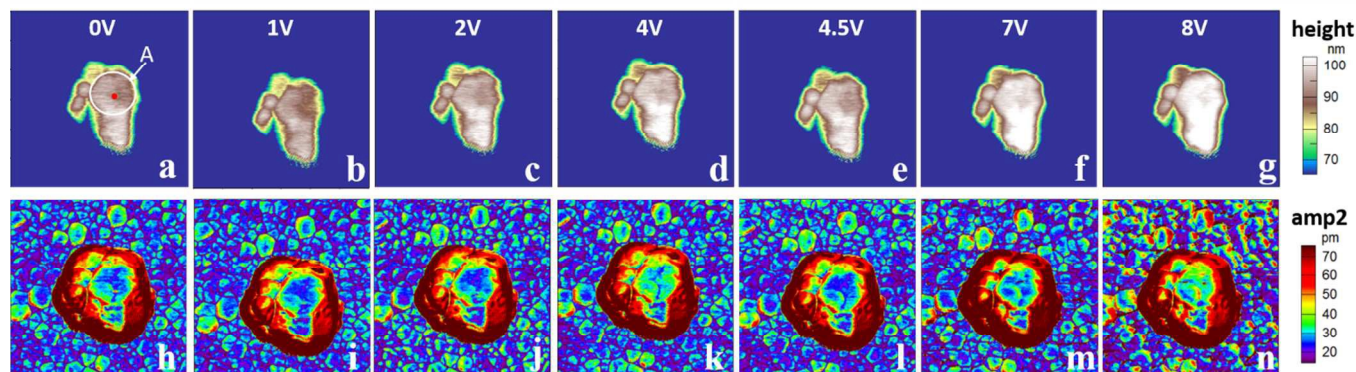

Figure 5. Topography and compositional variations of the LR nanoparticle observed by Bimodal-AM (phase1 < 90°) in Ar atmosphere. Scan size is 600×600 nm^2. A2 images were corrected by a factor as that in Figure 4 to maintain the same mean response of Pt-substrate. Bias was applied at the red-dot position inside region-A .
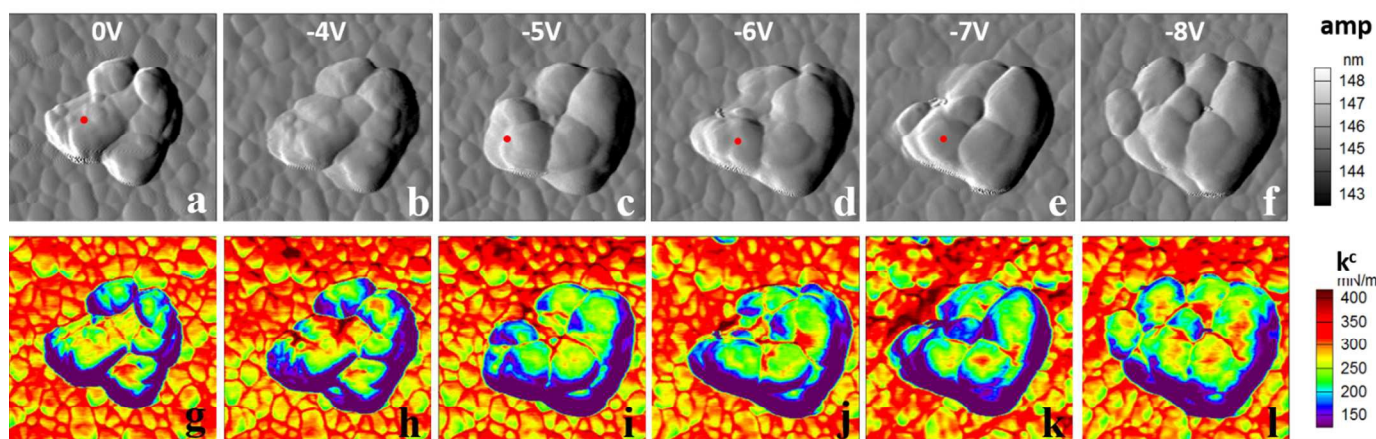

Figure 6. Morphology and stiffness variations of the LR particle triggered by escalating negative biases in the ambient air. Bias was applied from -1 to -8 V with increment of -1 V. The bias was applied the red dot for 30-second. Scan size is 400×400 nm^2. Stiffness images were also corrected based on the stiffness of Pt.

biases less negative than -4 V implies the intercalation may not or only minimally triggered due to the limited source of Li$^+$-ion in the particles. However, at large negative bias, electrons may be injected to the particle, which changes electronic interaction and hybridization that lead to phase transformation and distortion in lattice. Unlike positive voltage, long-hold negative voltage leads to coalescence of nanograins (possibly in different crystal orientation) into a larger particle and significant volume expansion. Li$^+$-ions may migrate to the grain boundaries and phase transformation may occur simultaneously. Again, such behaviours are also attributed to the moisture content. In SA, particle morphology did not change at -6 V, but suddenly fractured at -7 V (Fig.S7 – Supporting Information).

4. Summary, Implication and Conclusions

In this work, the electrochemical responses of the individual nanosize cathode particles are studied using the SPM-based techniques. The results from SPM study correlate well with the macroscopic electrochemical characteristics measurement. For example, the 1st charge/discharge curve shows a voltage plateau at ~ 4.5 V, at which the SPM measurements also show dramatic volume and morphology changes. Furthermore, at ~ 4V (corresponding to -4 V in the measurement by sample bias), significant current peaks also appears. Those current peaks may be related to the possible phase transformation at these voltage levels. In addition, the SPM results suggest that certain amount of Li$^+$-ions must be maintained inside the particle, otherwise particle may suffer from dramatic mechanical failure such as fracture. On the other hand, according to Fig.S1(b), the first fully charged capacity is 305 mAh/g. The theoretical capacity of LR particles when fully charged is 377 mAh/g, corresponds to a removal of 1.2 Li per formula unit. Therefore, the 305 mAh/g charged capacity is a consequence of 0.97 Li$^+$ removal, leading to Li$_{0.23}$Mn$_{0.54}$Ni$_{0.13}$Co$_{0.13}$O$_2$ as the final product. Although the exact Li$^+$ concentration during the intermediate bias applications

is unmeasurable, however, if assuming that the applied voltage by SPM conducted a similar removal effect of Li^+ on the single particle as those in the electrochemical charge/discharge measurements, then it is likely the lowest Li^+ concentration per formula unit is 0.23.

On the other hand, the SPM measurements are significantly different from the macroscopic electrochemical measurement. In this study, the SPM measurement is only conducted in single cathode particles, it is different from the measurement performed on a full or half battery structures. Therefore, the Li^+ ion movement is most likely constrained within the particles. Some domains or clusters may increase the Li^+-concentration whereas some others may decrease due to the redistribution of the Li^+ ions in the particles. However, it can be speculate that the concentration of the Li^+ has its limits because of the storage capability of the crystal structures of the materials. Another major limitations of the SPM method is that the newly formed phase or chemical composition in the particles cannot be differentiated unambiguously based on the structural difference; and therefore the Li^+ concentration in the particles cannot be directly determined from the SPM measurements. These information may be obtained by other in-situ techniques such as in-situ TEM or Raman spectroscopy, but combining those in-situ characterizations with SPM measurement is still a very challenging issue and worthwhile for future development.

In conclusion, this paper has presented a new approach and perspective to characterize single nanoparticle of, but not limited to, the Li-rich layered-oxide cathode using SPM-based techniques. The electric bias induced changes of morphology, elasticity, composition and conductivity for representative particles are observed and discussed. Higher electric bias is also applied to study the extreme state (fracture) of the LIB particles. The ratios of the reduced elastic modulus between LMO-like and NCM phases in pristine LR particles are quantified experimentally, in which suggests that high Li^+-ion concentration may lead to high stiffness. This observation also agrees with the theoretical and computational simulations. Comparing to that of the NCM and LMO nanoparticles, LR nanoparticles show morphological instability and complex conductivity fluctuation in air when applied bias is higher than 4 V, at which continuous phase transformation may occur. I-V curves reveal obvious differences in EC reaction mechanisms between the LR and NCM particles. Water molecules in air play a critical role to facilitate the EC reactions of the LR particles, so that excess Li^+-ions can be removed from the particle and causes significant morphology change, phase transformation and instability. Overall-speaking, this work provides insights of the qualitative and semi-quantitative responses of isolated active particles and hence sheds light on understanding the intrinsic characteristics of the active components in the electrodes for Li-ion battery. Finally, it also demonstrates the viable applications of multi-frequency SPM techniques to LIB research.

Acknowledgements

Notes

1. *Department of Mechanical Engineering, National University of Singapore, Engineering Drive 1, Singapore 117576.*
2. Current Address: *Department of Physics and Astronomy, University of Nebraska-Lincoln, Lincoln, NE 68588, USA.*
3. Current Address: *Department of Engineering Science, University of Oxford, Parks Road, Oxford OX1 3PJ, UK.*

* Corresponding author: *(Prof. Kaiyang Zeng, Tel: (+65) 6516 6627, fax: (+65) 6779 1459, E-mail: mpezk@nus.edu.sg*

† Electronic Supplementary Information (ESI) available: XRD pattern of the Li-rich particles; the first cycle of the charge/discharge curves for the Li-rich nanoparticles; averaged ratio of reduced elastic modulus between the LMO and NCM nanoparticles; stiffness variations of the Pt-substrate after applying long-hold voltage to Li-rich particle; volume evolution of LR nanoparticle induced by long-hold positive voltages in ambient air; bimodal-AM imaging of NCM particles in ambient air; bimodal-AM imaging of LMO particles in ambient air; Amplitude2 (A2) and phase2 images of the Pt-substrate versus voltage in synthetic air; bimodal-AM images of Li-rich nanoparticle in synthetic air; specifications of a typical SPM probe (AC240TM, Olympus, Japan) used in this work, calibrated by the GetReal™ software developed by Asylum Research (USA). See DOI: 10.1039/b000000x/

References

1. M. Hu, X. Pang and Z. Zhou, *J. Power Sources*, 2013, **237**, 229-242.
2. A. Mukhopadhyay and B. W. Sheldon, *Prog. Mater. Sci.*, 2014, **63**, 58-116.
3. H. Yu and H. Zhou, *J. Phys. Chem. Lett.*, 2013, **4**, 1268-1280.
4. Y.-K. Sun, Z. Chen, H.-J. Noh, D.-J. Lee, H.-G. Jung, Y. Ren, S. Wang, C. S. Yoon, S.-T. Myung and K. Amine, *Nat. Mater.*, 2012, **11**, 942-947.
5. M. S. Whittingham, *MRS Bull.*, 2008, **33**, 411-419.
6. M. Sathiya, G. Rousse, K. Ramesha, C. P. Laisa, H. Vezin, M. T. Sougrati, M. L. Doublet, D. Foix, D. Gonbeau, W. Walker, A. S. Prakash, M. Ben Hassine, L. Dupont and J. M. Tarascon, *Nat. Mater.*, 2013, **12**, 827-835.
7. D. Mohanty, A. S. Sefat, S. Kalnaus, J. Li, R. A. Meisner, E. A. Payzant, D. P. Abraham, D. L. Wood and C. Daniel, *J. Mater. Chem. A*, 2013, **1**, 6249-6261.
8. N. Balke, S. Jesse, A. N. Morozovska, E. Eliseev, D. W. Chung, Y. Kim, Adamczyk L., R. E. Garcia, N. Dudney and S. V. Kalinin, *Nat. Nanotechnol.*, 2010, **5**, 749-754.
9. X. Zhu, C. S. Ong, X. Xu, B. Hu, J. Shang, H. Yang, S. Katlakunta, Y. Liu, X. Chen, L. Pan, J. Ding and R.-W. Li, *Sci. Rep.*, 2013, **3**, 1084.
10. K. Dokko, M. Mohamedi, Y. Fujita, T. Itoh, M. Nishizawa, M. Umeda and I. Uchida, *J. Electrochem. Soc.*, 2001, **148**, A422-A426.
11. K. Dokko, M. Mohamedi, M. Umeda and I. Uchida, *J. Electrochem. Soc.*, 2003, **150**, A425-A429.

Physical Chemistry Chemical Physics Accepted Manuscript

This journal is © The Royal Society of Chemistry 20xx

Phys. Chem. Chem. Phys., 20xx, **00**, 1-8 | **7**

12. K. Zhao, M. Pharr, J. J. Vlassak and Z. Suo, *J. Appl. Phys.*, 2010, **108**, 073517.

13. R. Deshpande, Y.-T. Cheng, M. W. Verbrugge and A. Timmons, *J. Electrochem. Soc.*, 2011, **158**, A718-A724.

14. R. Garcia and E. T. Herruzo, *Nat. Nanotechnol.*, 2012, **7**, 217-226.

15. R. Garcia and R. Proksch, *Eur. Polym. J.*, 2013, **49**, 1897-1906.

16. S. D. Solares and G. Chawla, *J. Appl. Phys.*, 2010, **108**, 054901.

17. D. Ebeling and S. D. Solares, *Beilstein J. Nanotechnol.*, 2013, **4**, 198-207.

18. R. Garcia, R. Magerle and R. Perez, *Nat. Mater.*, 2007, **6**, 405-411.

19. N. F. Martinez, S. Patil, J. R. Lozano and R. Garcia, *Appl. Phys. Lett.*, 2006, **89**, 153115.

20. R. Proksch, *Appl . Phys. Lett.*, 2006, **89**, 113121.

21. N. Yabuuchi, K. Yoshii, S.-T. Myung, I. Nakai and S. Komaba, *J. Am. Chem. Soc.*, 2011, **133**, 4404-4419.

22. C. R. Fell, D. Qian, K. J. Carroll, M. Chi, J. L. Jones and Y. S. Meng, *Chem. Mater.*, 2013, **25**, 1621-1629.

23. P. He, H. Yu, D. Li and H. Zhou, *J. Mater. Chem.*, 2012, **22**, 3680-3695.

24. T. R. Rodríguez and R. García, *Appl. Phys. Lett.*, 2004, **84**, 449-451.

25. D. Kiracofe, A. Raman and D. Yablon, *Beilstein J. Nanotechnol* 2013, **4**, 385-393.

26. I. Chakraborty and D. G. Yablon, *Nanotechnology*, 2013, **24**, 1-7.

27. G. Chawla and S. D. Solares, *Appl. Phys. Lett.*, 2011, **99**, 074103.

28. M. M. Thackeray, S.-H. Kang, C. S. Johnson, J. T. Vaughey, R. Benedek and S. A. Hackney, *J. Mater. Chem.*, 2007, **17**, 3112-3125.

29. U. Rabe, S. Amelio, E. Kester, V. Scherer, S. Hirsekorn and W. Arnold, *Ultrasonics*, 2000, **38**, 430-437.

30. D. C. Hurley, in *Applied Scanning Probe Methods XI: Scanning Probe Microscopy Techniques*, eds. B. Bhushan and H. Fuchs, Springer, Heidelberg, 2009, pp. 97-138.

31. J. G. Swallow, W. H. Woodford, F. P. McGrogan, N. Ferralis, Y.-M. Chiang and K. J. Van Vliet, *J. Electrochem. Soc.*, 2014, **161**, F3084-F3090.

32. K. L. Duncan, Y. Wang, S. R. Bishop, F. Ebrahimi and E. D. Wachsman, *J. Am. Ceram. Soc.*, 2006, **89**, 3162-3166.

33. Y. Qi, L. G. Hector, C. James and K. J. Kim, *J. Electrochem. Soc.*, 2014, **161**, F3010-F3018.

34. D. Mohanty, S. Kalnaus, R. A. Meisner, A. S. Safat, J. Li, E. A. Payzant, K. Rhodes, I. I. I. D. L. Wood and C. Daniel, *RSC Adv.*, 2013, **3**, 7479-7485.

35. N. Balke, S. Kalinin, A. Morozovska and E. Eliseev, *J. Appl. Phys.*, 2010, **108**, 053712.

36. Q. Nataly Chen, Y. Liu, Y. Liu, S. Xie, G. Cao and J. Li, *Appl. Phys. Lett.*, 2012, **101**, 063901.

37. B. Song, M. O. Lai, Z. Liu, H. Liu and L. Lu, *J. Mater. Chem. A*, 2013, **1**, 9954-9965.

38. B. Xu, C. R. Fell, M. Chi and Y. S. Meng, *Energy Env. Sci.*, 2011, **4**, 2223-2233.

39. J. Hong, H.-D. Lim, M. Lee, S.-W. Kim, H. Kim, S.-T. Oh, G.-C. Chung and K. Kang, *Chem. Mater.*, 2012, **24**, 2692-2697.

40. M. Gu, I. Belharouak, J. Zheng, H. Wu, J. Xiao, A. Genc, K. Amine, S. Thevuthasan, D. R. Baer, J.-G. Zhang, N. D. Browning, J. Liu and C. Wang, *ACS Nano*, 2012, **7**, 760-767.

Physical Chemistry Chemical Physics Accepted Manuscript

8 | *Phys. Chem. Chem. Phys.*, 20xx, **00**, 1-8

This journal is © The Royal Society of Chemistry 20xx